Available online at http://jprm.sms.edu.pk/
Journal of Prime Research in Mathematics, 22(2) (2026), 18–32

Journal of Prime Research in Mathematics

Mathematical Modeling of COVID-19: Stability Analysis and Numerical Simulation

Ruchi Kaur[a,*], Prabhanshi[a], Ishita Jhamb[a]

[a] *Department of Mathematics, Sri Guru Tegh Bahadur Khalsa College, University of Delhi, Delhi-110007, India*

Abstract

COVID-19 has highlighted the critical role of population mobility and regional interactions in shaping the dynamics of infectious diseases.This study proposes a nonlinear model depicting the dynamics of the coronavirus, specifically accounting for behavioral heterogeneity between resident and visitor populations. R_0, (the basic reproduction number) is determined as it is the main determining parameter to analyze the dynamics of the disease. Stability analysis reveals that the disease-free- equilibrium is globally asymptotically-stable when $R_0 < 1$. For $R_0 > 1$, the global asymptotic stability of the endemic- equilibrium is established using a Lyapunov function. Furthermore, sensitivity analysis is performed to find the key parameters driving the progression of the pandemic. Numerical simulations are presented with available parametric values to validate the theoretical findings, providing insights into the interpretations that can be drawn about the dynamics of the disease.

Keywords: COVID-19, reproduction number, equilibrium point, stability analysis, numerical simulation.
2020 Mathematics Subject Classification : 92B05, 37N25, 34A30, 34D99

1. Introduction

The field of mathematical modeling has been recognized as an effective decision-making tool for analyzing the dynamics of spread and progression of infectious diseases and thereby guiding control mechanisms for the spread [16, 12]. Different models have been proposed based on the nature of the disease and the analytical and computational study of these models can contribute significantly towards control of the disease and prevention of its subsequent outbreaks [10, 3]. Since infectious diseases differ significantly in their biological and epidemiological characteristics, it is essential that mathematical models are formulated in a manner that adequately captures the underlying transmission mechanisms and population behavior [4, 19].
The COVID-19 pandemic, came into being in the last lap of the year 2019 and very rapidly turned into a global threat to public health. Following its initial detection in Wuhan, China [26], the disease spread across

*Corresponding author
Email addresses: ruchi@sgtbkhalsa.du.ac.in (Ruchi Kaur), prabhanshi.gaur@gmail.com (Prabhanshi), ishita.jhamb@gmail.com (Ishita Jhamb)

Received : 04 February 2026*; Accepted:* 20 May 2026*; Published Online:* 10 June 2026

continents within a couple of months which forced the global health organization; the WHO to announce this infection as a pandemic in March 2020.

The early phase of the pandemic was characterized by rapid transmission, limited clinical understanding, and the absence of pharmaceutical interventions [13]. As the outbreak progressed, extensive epidemiological data became available, allowing researchers to retrospectively analyze transmission patterns, intervention strategies, and population-level responses [27].

Clinical observations revealed substantial heterogeneity in disease outcomes. Although a large proportion of infected individuals experienced mild to moderate symptoms, severe complications such as acute respiratory distress syndrome were observed, particularly among elderly individuals and those with comorbidities. Over time, improvements in clinical management, widespread adoption of interventions such as isolation, use of protective facial masks, social distancing, and the launch of vaccination programs significantly reduced disease severity and mortality rates [23, 30]. These developments underscore the importance of incorporating evolving public health measures and population mobility into mathematical models of disease transmission [5].

The scale of spread of this pandemic stimulated a dire need for an extensive and deep research across various disciplines, with mathematical modeling emerging as a central tool for analyzing disease spread and assessing control strategies [6]. Numerous compartmental and data-driven models were proposed to study different aspects of the pandemic. Discrete-time and continuous-time models were developed to predict infection trajectories under quarantine and lockdown measures [18], while deterministic models calibrated with real-time data were used to estimate key epidemiological parameters.

Models involving fractional ordered derivatives [24] have been proposed and studied to catch hold of the dynamics of the pandemic through numerical and analytical approaches [1]. Other studies incorporated heterogeneous transmission mechanisms, including the role of super-spreader individuals, and explored hybrid approaches combining classical compartmental modeling with machine learning techniques for short-term forecasting.

Certainly, the technique of mathematical modeling has proved instrumental in analyzing the trajectories of infectious diseases like COVID-19. However in majority of the models considered in the existing literature, the infected population is assumed as a homogeneous group or it focuses primarily on closed systems. Current models frequently overlook the behavioral and epidemiological differences between local residents and incoming travelers, as well as the potential for transmission within treatment or quarantine settings. Despite the use of advanced techniques such as fractional derivatives to capture memory effects, there remains a critical gap in modeling scenarios where disease importation by visitors significantly alters regional transmission dynamics. Specifically, most SEIR-type models do not explicitly distinguish between resident-driven and visitor-driven infection or account for "hospital-acquired" or "quarantine-based" transmission from those already under treatment.

This study addresses these deficiencies by proposing a novel, modified SEIR framework [14] that incorporates heterogeneous infectious compartments explicitly separating resident ($\bar{I}_r$) and visitor ($\bar{I}_{or}$) infection pathways to reflect behavioral heterogeneity and varying isolation protocols. The model also considers the infectiousness of individuals under treatment or quarantine ($\bar{T}$) to model real-world risks of healthcare-associated clusters. To sum up, the proposed model accounts for a combination of population mobility and multi-stage treatment rates in a unified system to provide a more realistic description of post-lockdown regional dynamics. This formulation enables a clearer representation of disease importation and local transmission following the incubation period, thereby providing a more realistic description of regional disease dynamics. Such an approach is especially relevant for understanding post-lockdown mobility, inter-regional travel, and their long-term implications for epidemic control. The present work is compiled as follows: Section 1 is introductory, after which the next section, Section 2 talks about the formulation and background of the proposed mathematical model. Section 3 consists of a discussion on the well-posedness of the model. Sections 4 and 5 deal with the local- and global-type stability criteria for the disease-free and endemic-equilibria. Numerical simulations are presented in Section 6 and the sensitivity analysis in Section 7, to present the illustrations that validate the analytical findings. Finally, Section 8 concludes the works with a

brief discussion and remarks.
The model considered in this study is developed by the authors as a modified SEIR-type framework. While it is motivated by classical compartmental models available in the literature, yet it is a novel formulation where aspects of population mobility and treatment-based transmission is incorporated in a unified manner.

2. Mathematical Model: Background and Formulation

This section focuses on the mathematical formulation of a model to analyze the progression of COVID-19 infection within any particular region.
For this, we have divided the human population into six different heads. $\bar{S}(t)$: susceptible, is the part of the population that is prone to acquire infection from the infective that is currently residing in that region; $\bar{E}(t)$ is the exposed class of individuals who have caught the infection and are in their incubation period, but cannot spread the disease. The infectious population is divided into two categories, one is $\bar{I}_r(t)$;the class of infected human population already residing inside that region, and the other class is $\bar{I}_{or}(t)$ from which are the infected humans whose travel history was traced back to prove that they have traveled outside the region and arrived as infected; $\bar{T}(t)$ is a combined class of individuals who where either hospitalized or quarantined and they are under treatment; lastly, is the class of the recovered individuals denoted by $\bar{R}(t)$. Therefore the total human population $\bar{N}(t)$ at any time 't', is given by the sum of all population categories, (i.e., $\bar{N}(t) = \bar{S}(t) + \bar{E}(t) + \bar{I}_r(t) + \bar{I}_{or}(t) + \bar{T}(t) + \bar{R}(t)$).

Throughout the paper, it is assumed that the exposed class ($\bar{E}$) consists of individuals who have invaded by the virus but as the virus incubates at this stage, so the exposed individual is not a carrier untill he progresses to the infectious class.The susceptible population $\bar{S}$ acquires infection through three distinct pathways (Resident, Visitor, and under treatment class) represented by the weighted transmission rates β_1, β_2, and β_3. To maintain the focus on the initial and peak dynamics of the regional spread, it is assumed that recovered population have become immune to the disease at least for a particular time period; hence they would not be considered as susceptible during that period.

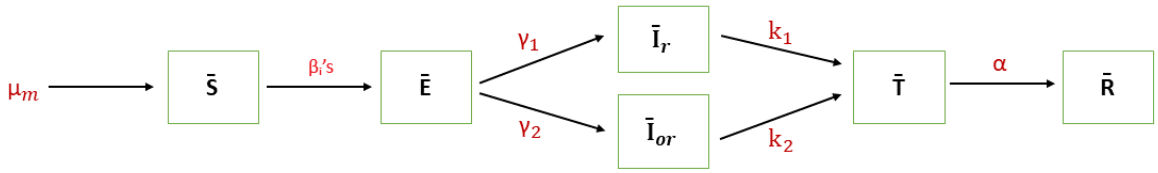

Figure 1: Flow diagram of disease progression.

Fig. 1 is the diagramatic representation showing the interaction between different categories of the population considered in the model. In this model, the infection to susceptible category is considered to be transmitted from the population categories, $\bar{I}_r$ (resident), $\bar{I}_{or}$ (visitor) and $\bar{T}$ with rates β_1, β_2, and β_3 respectively, therefore the rate shown on the arrow between $\bar{S}$ and $\bar{E}$ is shown by β_i in general, where $i = 1, 2, 3$. The distinction between $\bar{I}_r$ (resident) and $\bar{I}_{or}$ (visitor) is not merely based on origin but also accounts for behavioral heterogeneity. Visitors often exhibit different contact frequencies and have varying levels of access to local isolation protocols compared to established residents.
Furthermore, the infectiousness of the treated class T with parameter β_3 is included to account for hospital-acquired transmission, which has been identified as a critical factor in the regional amplification of COVID-19 clusters through healthcare [18, 21]. In addition, it is known that individuals who were quarantined in home

or in the hospital have been reported to spread the disease to others in close proximity to them.

Symbol	Description
μ_n	Natality rate
μ_m	Mortality rate
$\beta_1, \beta_2, \beta_3$	Rates of disease transmission to the susceptible class S from populations $\bar{I}_r$, $\bar{I}_{or}$ and T to the
γ_1, γ_2	Disease progression rate from E to $\bar{I}_r$ and $\bar{I}_{or}$ respectively.
k_1, k_2	Treatment rate for $\bar{I}_r$ and $\bar{I}_{or}$ sections of population.
α	Recovery rate of human population under treatment.

Table 1: List of parameteric rates of the model along with their description.

After a while, the susceptible individuals who had caught the infection and are carrying it asymptomatically finally move to the compartment $\bar{E}$. When their symptoms are prominent, they will be considered progressing to compartments $\bar{I}_r$ and $\bar{I}_{or}$, with the corresponding rate γ_1 if they had been in the exposed stage within the region and γ_2 if exposed outside the region respective;y.
After the diagnosis of the infected individual and tracing its travel history, the population will be classified into $\bar{I}_r$ or $\bar{I}_{or}$, which then undergoes treatment $\bar{T}$ with transmission rates k_1 or k_2 respectively. Finally, α is taken as the rate of individuals who move towards recovery $\bar{R}$.

Compiling the above discussion, the model is now mathematically formulated by the system of following ODE's:

$$\left.\begin{aligned}
\frac{d\bar{S}}{dt} &= \mu_n - \frac{\bar{S}}{\bar{N}}(\bar{P}) - \mu_m \bar{S}, \\
\frac{d\bar{E}}{dt} &= \frac{\bar{S}}{\bar{N}}(\bar{P}) - a_1 \bar{E}, \\
\frac{d\bar{I}_r}{dt} &= \gamma_1 \bar{E} - a_2 \bar{I}_r, \\
\frac{d\bar{I}_{or}}{dt} &= \gamma_2 \bar{E} - a_3 \bar{I}_{or}, \\
\frac{d\bar{T}}{dt} &= k_1 \bar{I}_r + k_2 \bar{I}_{or} - a_4 \bar{T}, \\
\frac{d\bar{R}}{dt} &= \alpha \bar{T} - \mu_m \bar{R}.
\end{aligned}\right\} \tag{2.1}$$

where, $\bar{P} = \beta_1 \bar{I}_r + \beta_2 \bar{I}_{or} + \beta_3 \bar{T}$,
$a_1 = \gamma_1 + \gamma_2 + \mu_m$,
$a_2 = k_1 + \mu_m$,
$a_3 = k_2 + \mu_m$,
$a_4 = \alpha + \mu_m$,
The model introduced through the above discussion is a modification of standard SEIR-type models, for-

mulated to capture heterogeneity in infection sources through separate infectious classes and to account for transmission from individuals under treatment.

3. Well-posedness.

3.1. Positivity

This section deals with the analysis of the elementary properties of solutions associated with model (1). The variables of the model are shown to be non-negative, thereby establishing the epidemiological validity of the model in discussion [2].

Lemma 1: The solution $\bar{Y}(t) = (\bar{S}, \bar{E}, \bar{I}_r, \bar{I}_{or}, \bar{T}, \bar{R})$, is non-negative whenever $t > 0$ where the annexed underlying condition is $\bar{Y}(0) > 0$.

Proof: Let t_1 = supremum of the set $\{t : \bar{Y}(t) > 0\} > 0$. Then, for the following equation from (1),

$$\frac{d\bar{S}}{dt} = \mu_n - \frac{\bar{S}}{\bar{N}}(P) - \mu_m \bar{S},$$

solution is given by:

$$\frac{d}{dt}\left\{\bar{S}(t)\exp\left[\int_0^{t_1}\frac{\bar{P}(\theta)}{\bar{N}(\theta)}d\theta + \mu_m t\right]\right\} = \mu_n \exp\left[\int_0^{t_1}\frac{\bar{P}(\theta)}{\bar{N}(\theta)}d\theta + \mu_m t\right]$$

which implies

$$\bar{S}(t_1)\exp\left[\int_0^{t_1}\frac{\bar{P}(\theta)}{\bar{N}(\theta)}d\theta + \mu_m t_1\right] - \bar{S}(0) = \int_0^{t_1}\mu_n \exp\left[\int_0^{u}\frac{\bar{P}(\theta)}{\bar{N}(\theta)}d\theta + \mu_m u\right]du.$$

Furthermore,

$$\begin{aligned}\bar{S}(t_1) = \bar{S}(0)\exp\left[-\int_0^{t_1}\frac{\bar{P}(\theta)}{\bar{N}(\theta)}d\theta + \mu_m t_1\right] \\ + \exp\left[\left(-\int_0^{t_1}\frac{\bar{P}(\theta)}{\bar{N}(\theta)}d\theta + \mu_m t_1\right)\right] \times \int_0^{t_1}\mu_n \exp\left[\int_0^{t_1}\frac{\bar{P}(\theta)}{\bar{N}(\theta)}d\theta + \mu_m u\right]du > 0.\end{aligned}$$

Likewise, positivity of all the other variables of system (1) can be established and hence $\bar{Y}(t) > 0$ for all $t > 0$.

3.2. Invariance

The closed set:

$$\psi = \{(\bar{S}, \bar{E}, \bar{I}_r, \bar{I}_{or}, \bar{T}, \bar{R}) \in \mathbb{R}^6_+ : \bar{N}(t) \leq \frac{\mu_n}{\mu_m}\}$$

(where $\bar{N}(t)$ is the sum of the six compartments sted above) is positively-invariant ensuring that any non-negative solution from the region ψ, satisfying the annexed conditions will retain its sign for each $t > 0$ [22].

Lemma 2: The feasible region ψ in $\mathbb{R}^6_+$ is positively-invariant along with the annexed initial conditions as non-negative. In addition, $\sup \bar{N}(t) \to \dfrac{\mu_n}{\mu_m}$ as $t \to \infty$.

Proof: Adding the equations of system (1), we get

$$\begin{aligned}\frac{d\bar{N}}{dt} &= \mu_n - \mu_m(\bar{S} + \bar{E} + \bar{I}_r + \bar{I}_{or} + \bar{T} + \bar{R}) \\ &\leq \mu_n - \mu_m(\bar{N})\end{aligned}$$

Integrating the inequality $\dfrac{d\bar{N}}{dt} \leq \mu_n - \mu_m\bar{N}$, gives $\bar{N}(t) \leq \bar{N}(0)\exp[-\mu_m t] + \dfrac{\mu_n}{\mu_m}\left(1 - \exp[-\mu_m t]\right)$, whenever $t \geq 0$. Additionally, $\lim\limits_{t\to\infty}\bar{N}(t) = \dfrac{\mu_n}{\mu_m}$. Hence $0 < \lim\limits_{t\to\infty}\sup\bar{N}(t) \leq \dfrac{\mu_n}{\mu_m}$. Hence, for the model in discussion, all solutions in $\mathbb{R}^6_+$ will be always contained in ψ, implying that ψ a positively-invariant set.

3.3. Uniqueness

Lemma 3: For any initial data $\bar{Y}(0)$ starting in the feasible region ψ, a unique solution $\bar{Y}(t)$ exists for the considered model (1), for each $t > 0$. Furthermore, this solution remains in ψ and is continuously dependent on the initial data, $\bar{Y}(0)$.

Proof. Let $\frac{d\bar{Y}}{dt} = f(\bar{Y})$ where $\bar{Y} = (\bar{S}, \bar{E}, \bar{I}_r, \bar{I}_{or}, \bar{T}, \bar{R}) \in \psi$. Since the components of the vector field $f(\bar{Y})$ are continuously differentiable, it follows that f is locally Lipschitz continuous on the domain ψ. The Picard-Lindelöf theorem [29] ensures the existence of the unique solution $\bar{Y}(t)$ that satisfies the initial condition $\bar{Y}(0) \in \psi$. As already seen, ψ is positively-invariant and the solutions are bounded ($\bar{N}(t) \leq \mu_n/\mu_m$), the local solution is extendable for all $t > 0$. The Lipschitz continuity further ensures that the solution operator $\Phi_t(\bar{Y}_0) = \bar{Y}(t)$ is continuous implying that the model is well-posed.

4. Disease-Free-Equilibrium (D-F-E)

This section discusses the local- and global- type stability for the uniquely existing D-F-E.

4.1. Existence of D-F-E

Disease-Free-Equilibrium (D-F-E) is referred to the point of the feasible region where population in consideration is completely free from infection. Let $E_0 = (S^*, E^*, I_r^*, I_{or}^*, T^*, R^*)$ denote the the D-F-E for model (1). As $\bar{S}$ and $\bar{R}$ are the only disease- free compartments, therefore $E_0 = (S^*, 0, 0, 0, 0, R^*)$.
Assigning value zero to all the variables of (1) other than $\bar{S}$ and $\bar{R}$ and solving for the two by equating their derivative values to zero, the D-F-E point is obtained as

$$E_0 = \left(\frac{\mu_n}{\mu_m}, 0, 0, 0, 0, 0\right).$$

4.2. Reproduction Number

Let R_0 denote the reproduction number for model (1), which in simply words is understood as the estimated number of individuals acquiring infection in an entirely disease-free population by introduction of a single infective carrier.
R_0, mathematically is the most positive eigen value of an associated matrix G which is obtained by multiplying the matrices as $F * V^{-1}$, with $F = \frac{\partial \mathcal{F}_i(E_0)}{\partial(x_j)}$ and $V = \frac{\partial \mathcal{V}(E_0)}{\partial(x_j)}$ for $1 \leq i, j \leq 4$.
For each i here, $\mathcal{F}_i(x)$ denotes the rate at which the new and fresh infection appears in each of the compartments and, $\mathcal{V}_i(x)$ takes into account, the final transmission of disease in the corresponding segments. The next-generation-matrix is denoted by G which is evaluated by matrix multiplication of F and V^{-1}.
Now decomposing the RHS of equations in (1) for compartments with infection, namely $\bar{E}, \bar{I}_r, \bar{I}_{or}$ and $\bar{T}$ in the above said manner, R_0 can be calculated.

$$\text{Clearly, } \mathcal{F} = \begin{bmatrix} \frac{\bar{S}}{\bar{N}}(\bar{P}) \\ 0 \\ 0 \\ 0 \end{bmatrix} \text{ and } \mathcal{V} = \begin{bmatrix} a_1\bar{E} \\ -\gamma_1\bar{E} + a_2\bar{I}_r \\ -\gamma_2\bar{E} + a_3\bar{I}_{or} \\ -k_1\bar{I}_r - k_2\bar{I}_{or} + a_4\bar{T} \end{bmatrix}.$$

For $x_j = (\bar{E}, \bar{I}_r, \bar{I}_{or}, \bar{T})$, computing the matrices F and V that are simply the Jacobians of the vectors $\mathcal{F}$ and $\mathcal{V}$, we get,

$$F = \frac{\partial \mathcal{F}(E_0)}{\partial x_j} = \begin{bmatrix} 0 & \beta_1 & \beta_2 & \beta_3 \\ 0 & 0 & 0 & 0 \\ 0 & 0 & 0 & 0 \\ 0 & 0 & 0 & 0 \end{bmatrix} \text{ and } V = \frac{\partial \mathcal{V}(E_0)}{\partial x_j} = \begin{bmatrix} a_1 & 0 & 0 & 0 \\ -\gamma_1 & a_2 & 0 & 0 \\ -\gamma_2 & 0 & a_3 & 0 \\ 0 & -k_1 & -k_2 & a_4 \end{bmatrix}.$$

Taking the largest eigen value of next- generation-matrix G as reproduction number, we have

$$R_0 = \frac{\beta_1(\gamma_1 a_3 a_4) + \beta_2(\gamma_2 a_2 a_4) + \beta_3(\gamma_1 a_3 k_1 + \gamma_2 a_2 k_2)}{a_1 a_2 a_3 a_4}$$

wherein as defined earlier in Section 2, $a_1 = \gamma_1 + \gamma_2 + \mu_m$, $a_2 = k_1 + \mu_m$,$a_3 = k_2 + \mu_m$ and $a_4 = \alpha + \mu_m$.

4.3. D-F-E: Local-Stability

The following section establishes the local-stability of the above mentioned D-F-E point ([9]).

Theorem 1: The Disease-Free-Equilibrium point (E_0) is l.a.st (locally-asymptotically-stable) whenever $R_0 \leq 1$ and is unstable if $R_0 > 1$.

Proof: The variational matrix $J(E_0)$ for the model is evaluated as the Jacobian of the system (1), given by

$$J(E_0) = \begin{bmatrix} -\mu_m & 0 & -\beta_1 & -\beta_2 & -\beta_3 & 0 \\ 0 & -a_1 & \beta_1 & \beta_2 & \beta_3 & 0 \\ 0 & \gamma_1 & -a_2 & 0 & 0 & 0 \\ 0 & \gamma_2 & 0 & -a_3 & 0 & 0 \\ 0 & 0 & k_1 & k_2 & -a_4 & 0 \\ 0 & 0 & 0 & 0 & \alpha & -\mu_m \end{bmatrix}.$$

Here, the trace of $J(E_0)$ is negative and determinant of this matrix [11], is given as follows:

$$|J(E_0)| = a_1 a_2 a_3 a_4 u_m^2 - a_3\beta_3\gamma_1 k_1 u_m^2 - a_2\beta_3\gamma_2 k_2 u_m^2 - a_3 a_4\beta_1\gamma_1 u_m^2 - a_2 a_4\beta_2\gamma_2 u_m^2$$

or

$$det(J(E_0)) = (a_1 a_2 a_3 a_4 - a_3\beta_3\gamma_1 k_1 - a_2\beta_3\gamma_2 k_2 - a_3 a_4\beta_1\gamma_1 - a_2 a_4\beta_2\gamma_2)u_m^2$$

Using the expression for R_0, derived above; clearly for $R_0 < 1$, we have:

$$a_3\beta_3\gamma_1 k_1 + a_2\beta_3\gamma_2 k_2 + a_3 a_4\beta_1\gamma_1 + a_2 a_4\beta_2\gamma_2 < a_1 a_2 a_3 a_4$$

Therefore,

$$a_1 a_2 a_3 a_4 - a_3\beta_3\gamma_1 k_1 - a_2\beta_3\gamma_2 k_2 - a_3 a_4\beta_1\gamma_1 - a_2 a_4\beta_2\gamma_2 > 0$$

or $det(J(E_0)) > 0$. Hence, the D-E-F E_0 is locally-asymptotically-stable whenever $R_0 < 1$.

4.4. Global-Stability

Next, the global-stability of D-F-E is examined for the proposed model. Rewriting model (1) as:

$$\left.\begin{aligned} \frac{d\bar{X}}{dt} &= \bar{F}(\bar{X}, \bar{Z}), \text{and} \\ \frac{d\bar{Z}}{dt} &= \bar{G}(\bar{X}, \bar{Z}), \qquad \bar{G}(\bar{X}, 0) = 0, \end{aligned}\right\} \tag{4.1}$$

where $(\bar{X}, \bar{Z}) \in \mathbb{R}^2 \times \mathbb{R}^4$, with $\bar{X} = \{\bar{S}, \bar{R}\} \in$ and $\bar{Z} = \{\bar{E}, \bar{I}_r, \bar{I}_{or}, \bar{T}\}$. Let $E_0^* = \left(\bar{X}^*, 0\right)$ represent the D-F-E of system (2), with $\bar{X}^* = \left(\frac{\mu_n}{\mu_m}, 0\right)$. To ensure the g.a.stability, the conditions (H1) and (H2) given below need to hold essentially [7]:

(H1) X^* must be g.a.st for $\frac{d\bar{X}}{dt} = \bar{F}(\bar{X}, 0)$, and

(H2) For the matrix, $\bar{A} = \frac{\partial \bar{G}(\bar{X}^*, \bar{Z})}{\partial \bar{Z}}$, with all off-diagonal entries as non-negative, $\hat{G}(\bar{X}, \bar{Z}) \geq 0$ whenever

$(\bar{X}, \bar{Z}) \in \psi$, the equation $\bar{G}(\bar{X}, \bar{Z}) = -\hat{G}(\bar{X}, \bar{Z}) + \bar{A}\bar{Z}$ must hold.

Theorem 2: The equilibrium point $E_0^* = (X^*, 0)$ is g.a.st if $R_0 < 1$.
Proof: As already proved in Theorem 1 that for $R_0 < 1$, E_0 is l.a.st. Solving the system

$$\frac{d\bar{X}}{dt} = \bar{F}(\bar{X}, 0) = \begin{bmatrix} \mu_n - \mu_m \bar{S} \\ 0 \end{bmatrix},$$

we get $\bar{S} = \frac{\mu_n}{\mu_m}[1 - \exp[-\mu_m t]]$. As $t \to \infty$, $\bar{S} = \frac{\mu_n}{\mu_m}$ and $\bar{R} = 0$. This implies that the point, $\bar{X}^*$ is a g.a.st equilibrium of $\frac{d\bar{X}}{dt} = \bar{F}(\bar{X}, 0)$ and hence (H1) is satisfied. Now,

$$\bar{G}(\bar{X}, \bar{Z}) = \begin{bmatrix} \frac{\bar{S}}{\bar{N}}(\beta_1 \bar{I}_r + \beta_2 \bar{I}_{or} + \beta_3 \bar{T}) - a_1 \bar{E} \\ \gamma_1 \bar{E} - a_2 \bar{I}_r \\ \gamma_2 \bar{E} - a_3 \bar{I}_{or} \\ k_1 \bar{I}_r + k_2 \bar{I}_{or} - a_4 \bar{T} \end{bmatrix}.$$

For (H2), consider $\bar{G}(\bar{X}, \bar{Z}) = -\hat{G}(\bar{X}, \bar{Z}) + \bar{A}\bar{Z}$, where

$$\bar{A} = \frac{\partial \bar{G}(\bar{X}^*, 0)}{\partial \bar{Z}} = \begin{bmatrix} -a_1 & \beta_1 & \beta_2 & \beta_3 \\ \gamma_1 & -a_2 & 0 & 0 \\ \gamma_2 & 0 & -a_3 & 0 \\ 0 & k_1 & k_2 & -a_4 \end{bmatrix}$$

.

$$\bar{A}\bar{Z} = \begin{bmatrix} -a_1 \bar{E} + \beta_{\bar{I}_s} \bar{I}_s + \beta_1 \bar{I}_r + \beta_2 \bar{I}_{or} + \beta_3 \bar{T} \\ \gamma_2 \bar{E} - a_3 \bar{I}_{or} \\ k_1 \bar{I}_r + k_2 \bar{I}_{or} - a_4 \bar{T} \end{bmatrix}.$$

As $\hat{G}(\bar{X}, \bar{Z}) = -\bar{G}(\bar{X}, \bar{Z}) + \frac{\partial \bar{G}(\bar{X}^*, 0)}{\partial Z} Z$, therefore

$$\hat{G}(\bar{X}, \bar{Z}) = \begin{bmatrix} \left(1 - \frac{\bar{S}}{\bar{N}}\right)(\beta_1 \bar{I}_r + \beta_2 \bar{I}_{or} + \beta_3 \bar{T})) \\ 0 \\ 0 \\ 0 \end{bmatrix}.$$

As, $1 - \frac{\bar{S}}{\bar{N}} > 0$ therefore (H2) holds. Hence the global-asymptotic-stability of $E_0^* = \left(\bar{X}^*, 0\right)$ is proved, provided $R_0 < 1$.

5. Endemic-Equilibrium (E-E)

The following section analyses the E-E point; its existence and its stability criterion.

5.1. Existence

The existence of a unique E-E-point, $E_e^* = (S^{**}, E^{**}, I_r^{**}, I_{or}^{**}, T^{**}, R^{**})$ for model (1) is ensured, provided $R_0 > 1$. To evaluate E_e^* [25], define

$$\kappa^* = \frac{P^{**}}{N^{**}} = \frac{1}{N^{**}}(\beta_1 I_r^{**} + \beta_2 I_{or}^{**} + + \beta_3 T^{**})$$

Expressing S^{**} in terms of κ^* and solving the simultaneous system (1) in terms of S^{**}, while equating RHS of each equation to zero,and substituting the value of in each of the subsequent equations, the following E-E point can be obtained:

$$S^{**} = \frac{\mu_n}{\mu_m + \kappa^*}$$
$$E^{**} = \frac{\mu_n \kappa^*}{a_1(\mu_m + \kappa^*)}$$
$$\bar{I}_r^{**} = \frac{\gamma_1 \mu_n \kappa^*}{a_1 a_2(\mu_m + \kappa^*)}$$
$$\bar{I}_{or}^{**} = \frac{\gamma_2 \mu_n \kappa^*}{a_1 a_3(\mu_m + \kappa^*)}$$
$$T^{**} = \frac{\mu_n \kappa^*(k_1 a_3 \gamma_1 + k_2 a_2 \gamma_2)}{a_1 a_2 a_3 a_4(\mu_m + \kappa^*)}$$
$$R^{**} = \frac{\mu_n \kappa^* \alpha(k_1 a_3 \gamma_1 + k_2 a_2 \gamma_2)}{a_1 a_2 a_3 a_4(\mu_m + \kappa^*)}$$

Substituting E_e^* in the expression for κ^*, shows that the following two equations are satisfied by the E-E point of (1):
$X\kappa^* - Y = 0$ with, $X\kappa^* = a_2a_3a_4 + \gamma_1 a_3 a_4 + \gamma_2 a_2 a_4 + (1+\alpha)(k_2 a_2 \gamma_2 + k_1 a_3 \gamma_1)$
and $Y = a_1 a_2 a_3 a_4 (R_0 - 1)$.
As all the constants in the above linear equation are positive, we get $X\kappa^* > 0$. Further, $Y > 0$ if and only if $R_0 > 1$. Hence, it can be concluded that the model (1) has a unique E-E point if $R_0 > 1$.

5.2. Local-Stability

Theorem 3: The Endemic-Equilibrium-Point E_e^* of model (1) is l.a.st if $R_0 > 1$.
Proof: The Jacobian matrix at E_e^*, denoted by $J_{E_e^*}$ for model (1) is given by

$$J_{E_e^*} = \begin{bmatrix} \theta_1 - \mu_m & \theta_2 & \theta_3 & \theta_4 & \theta_5 & \theta_2 \\ -\theta_1 & -\theta_2 - a_1 & -\theta_3 & -\theta_4 & -\theta_5 & -\theta_2 \\ 0 & \gamma_{I_1} & -a_2 & 0 & 0 & 0 \\ 0 & \gamma_{I_2} & 0 & -a_3 & 0 & 0 \\ 0 & 0 & k_1 & k_2 & -a_4 & 0 \\ 0 & 0 & 0 & 0 & \alpha & -\mu_m \end{bmatrix}.$$

where $\theta_1 = \frac{\kappa^* S^{**}}{\bar{N}^{**}} - \kappa^*$, $\theta_2 = \frac{\kappa^* S^{**}}{\bar{N}^{**}}$, $\theta_3 = \frac{\kappa^* S^{**}}{\bar{N}^{**}} - \frac{S^{**}\beta_1}{\bar{N}^{**}}$, $\theta_4 = \frac{\kappa^* S^{**}}{\bar{N}^{**}} - \frac{S^{**}\beta_2}{\bar{N}^{**}}$, $\theta_5 = \frac{\kappa^* S^{**}}{\bar{N}^{**}} - \frac{S^{**}\beta_3}{\bar{N}^{**}}$.

Clearly,the trace of the matrix $J_{E_e^*}$ is $-\kappa^* - a_1 - a_2 - a_3 - a_4 - 2\mu_m < 0$ and its determinant [28, 8] is given by:

$$det(J_{E_e^*}) = \frac{\mu_m^2 \mu_n \kappa^*}{\mu_m + \kappa^*}[a_1 a_2 a_3 a_4 (R_0 - 1) + X_1 + X_2 \mu_m)]$$

where $X_1 = \alpha(a_3 k_1 \gamma_1 + a_2 k_2 \gamma_2)$ and $X_2 = a_2 a_3 a_4 + \gamma_1 a_3 (a_4 + k_1)$
It can be observed that $det(J_{E_e^*}) > 0$ if $R_0 > 1$. Hence, the E-E point (E_e^*) is l.a.st provided $R_0 > 1$.

5.3. Global-Stability

Next, the global-asymptotic-stability of the E-E-point (E_e^*), is analyzed by considering a suitable Lyapunov function [17].
Theorem 4 *For $R_0 > 1$, the endemic- equilibrium-point, (E_e^*) of the system is globally-asymptotically-stable in the invariant region ψ.*

Proof. Consider the Lyapunov function $L : \psi \to \mathbb{R}$ as follows:

$$L = \frac{1}{2}\left[(\bar{S} - S^{**})^2 + (\bar{E} - E^{**})^2 + (\bar{I}_r - I_r^{**})^2 + (\bar{I_{or}} - I_{or}^{**})^2 + (\bar{T} - T^{**})^2 + (\bar{R} - R^{**})^2\right]$$

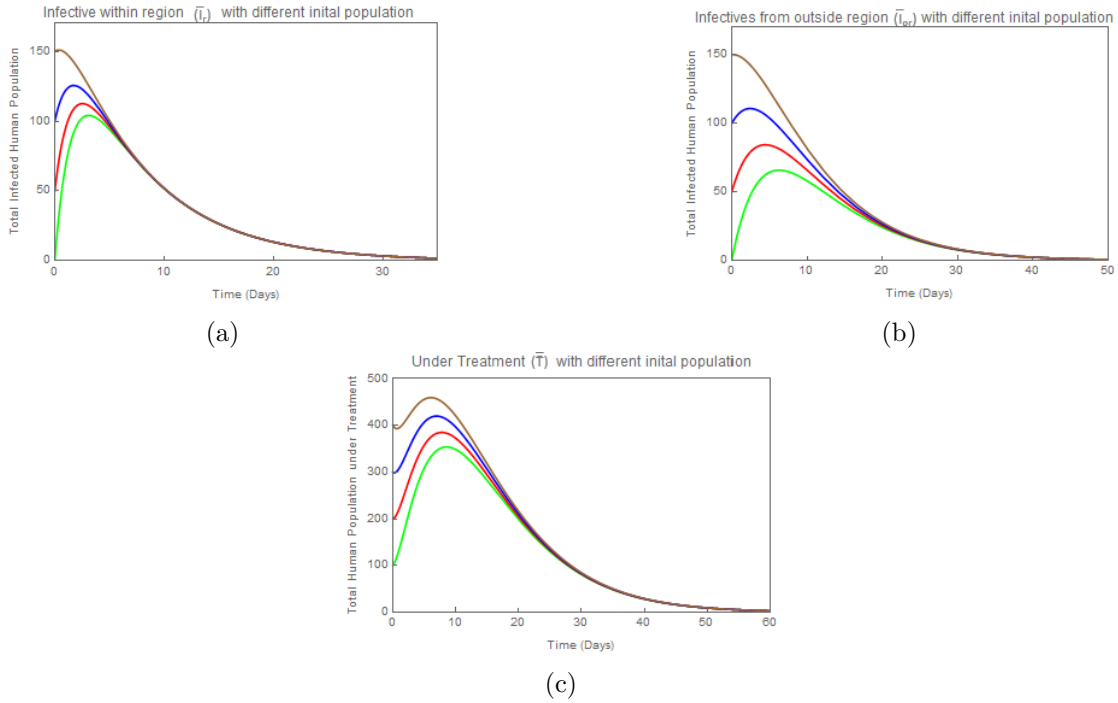

Figure 2: *Trajectory plots of various compartments when $R_0 > 1$, with different sets of initial conditions using the parametric values given in Table 2.*

Clearly, L is a positive definite function that vanishes only at the equilibrium point (E_e^*). Time derivative of L along the trajectories of the system yields:

$$\dot{L} = (\bar{S} - S^{**})\dot{S} + (\bar{E} - E^{**})\dot{E} + (\bar{I}_r - I_r^{**})\dot{I}_r + (\bar{I_{or}} - I_{or}^{**})\dot{I}_{or} + (\bar{T} - T^{**})\dot{T} + (\bar{R} - R^{**})\dot{R}$$

Substituting the expressions for $\dot{S}, \dot{E}, \ldots, \dot{R}$ from the system equations and linearizing around (E_e^*) using the Jacobian matrix A, we obtain:

$$\dot{L} = (\bar{x} - (E_e^*))^T A(\bar{x} - (E_e^*))$$

where $\bar{x} = (\bar{S}, \bar{E}, \bar{I}_r, \bar{I_{or}}, \bar{T}, \bar{R})^T$ and matrix A is the Jacobian of system (1) evaluated at the endemic-equilibrium (E_e^*). Since the real parts of eigenvalues of the matrix A are negative when $R_0 > 1$, therefore the quadratic form $(\bar{x} - (E_e^*))^T A(\bar{x} - (E_e^*))$ is negative semi-definite.

Furthermore, the set $\{x \in \psi : \dot{L} = 0\}$ contains only the singleton (E_e^*). Since the solutions are bounded within the region ψ, it follows from the LaSalle's Invariance Principle and the application of Barbalat's Lemma that every solution starting in ψ converges to (E_e^*) as $t \to \infty$. Thus, the endemic equilibrium is globally-asymptotically-stable. Further, the time derivative dL/dt remains negative definite within a neighborhood of the equilibrium, ensuring that the system's 'energy' dissipates as it converges to the steady state. □

6. Numerical Simulation

The graphical visualizations presented in this section will ensure the validation of the analytical results discussed in the above sections.Table 2 lists the parametric values that will be used throughout the simulation process.

Figure 3 shows the trajectory of different types of population compartments when $R_0 > 1$, (in particular when $R_0 = 4.57105$). From the graphs, it is evident that the infected population or patients undergoing some

Parameters	Value	Source
β_1	0.455	[20]
β_2	0.13	[20]
β_3	0.3506	[20]
γ_1	0.1	Assumed
γ_2	0.02857	Assumed
k_1	0.623	Assumed
k_2	0.178	Assumed
α	0.1358	Assumed
μ_n	0.01936	[15]
μ_m	0.00718	[15]

Table 2: Values of Parameters for Simulation

treatment will eventually move towards recovery. However, as per the assumptions of our model, eventually the recovered population becomes immune to the infection; therefore its graph (unlike other graphs) is well above the $x-$axis, maintaining a non-zero value for the entire time period in consideration. This goes in accordance with the underlying assumption that recovered population have become immune to the disease at least for a particular time period; hence they would not be considered as susceptible during that period. From Figure 2, we can infer that the number of infectives or patients undergoing treatment in a region, small or large, will surely recover in an estimated period of time with a prescribed rate, which goes well with the actual real-life scenario witnessed by the human population.

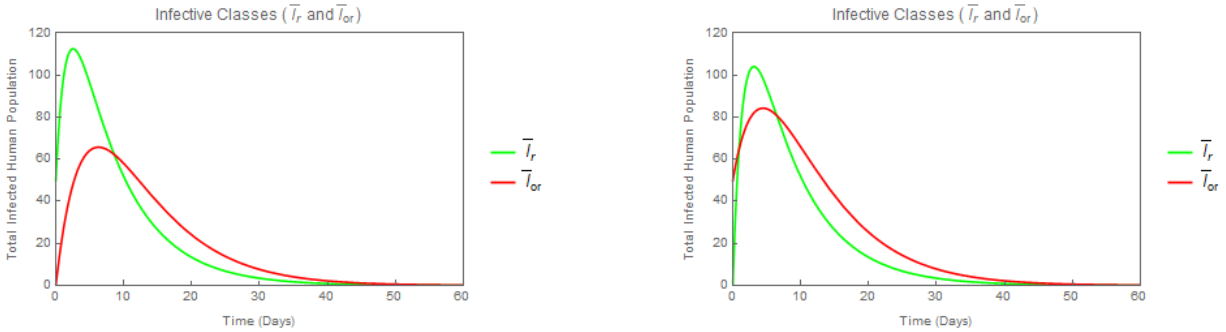

(a) (b)

Figure 4: *Trajectory plots of $\bar{I}_r$ and $\bar{I}_{or}$ for $R_0 > 1$ with different initial populations using parametric values given in Table 2.*

In an attempt to trace the origin of the spread of this disease, graphs with different underlying situations have been plotted (see Figure 4). In Figure 4(a), the situation considered is that $\bar{I}_{or}$ is taken to be zero, that is, if the cause of the outbreak of disease in the concerned region is presumed to be infectious individuals residing in the same region for 15 days or more. In contrast, in Figure 4(b), the situation considered was the other category of infected individuals, where it was assumed that the outbreak of infection is due to infectives who have recently joined the concerned region from a place outside its geographical boundary in the last two weeks.

Interestingly, in both situations, over a period of time, the curve representing the infected resident population surpasses the trajectory curve of visitor class of infected population. From these two graphs, it can be clearly concluded that $\bar{I}_r$ or $\bar{I}_{or}$, whatever the reason for the outbreak of infection in a region; once the infection hits the region, the spread would eventually become more prevalent at the local level. Additionally, as shown in Fig. 3, in due course of time, the infected population recovers if it is hospitalized or quarantine mode.

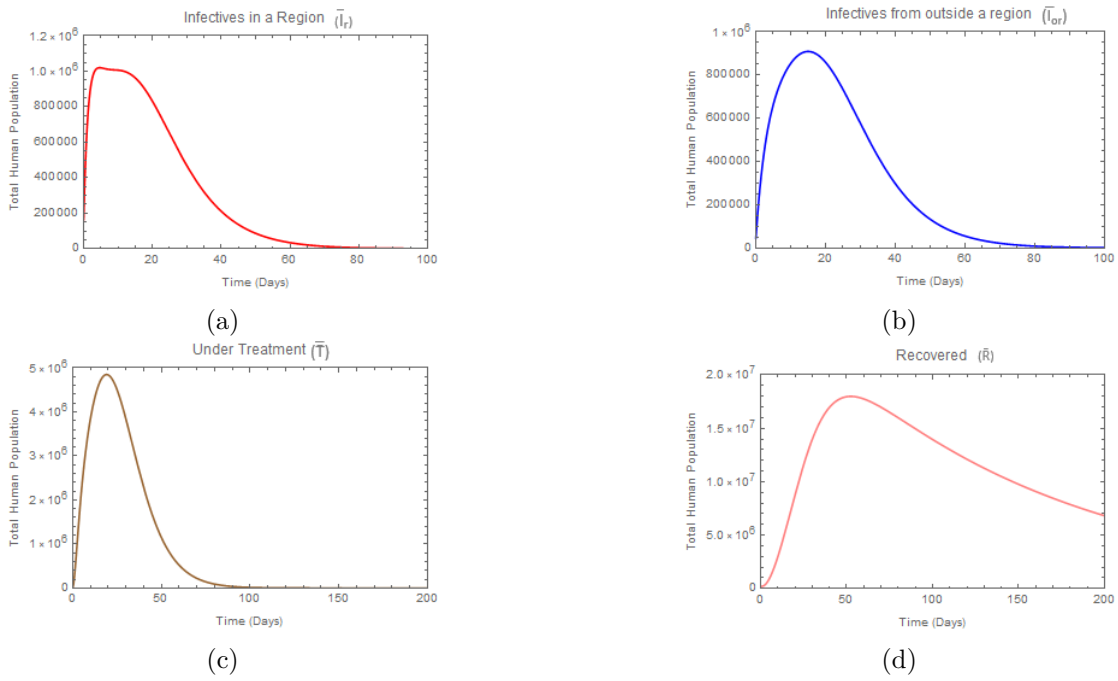

Figure 3: *Trajectory plots of various compartments when $R_0 > 1$, using the parametric values given in Table 2.*

The simultaneous system (1) was symbolically solved using Wolfram Mathematica. The simulations were carried out using the values of parameters as listed in Table 2, along with appropriate initial conditions for each compartment. The numerical solutions were obtained using standard built-in solvers, and the resulting trajectories were used to illustrate the dynamical behavior of the model.

7. Sensitivity Analysis

This section focuses on the determination of the relative effect of involved parameters on R_0. For any parameter p,the normalized forward sensitivity index of R_0 is given by:

$$S_p = \frac{\partial R_0}{\partial p} \cdot \frac{p}{R_0}.$$

The results in Table 3 show that R_0 is highly sensitive to β_3 and α, which exhibit the largest positive and negative sensitivity indices, respectively.

This highlights that transmission from treated individuals significantly drives the spread of infection, while increasing recovery rates plays a crucial role in mitigating disease transmission.

Parameter	β_1	β_2	β_3	γ_1	γ_2	k_1	k_2	α	μ_m
Sensitivity Sign	+ve	+ve	+ve	+ve	+ve	-ve	-ve	-ve	-ve
Sensitivity Value	0.1796	0.0499	0.7705	0.0460	0.0069	0.1707	0.0415	0.7318	0.1089

Table 3: Numerical values of sensitivity indices of R_0 with respect to different parameters

Figure 5 is a visualization of the sensitivity indices of R_0 with respect to the parameters involved. The positive value for the sensitivity indices corresponding to the transmission parameters β_1, β_2, indicates that with an increase in these parameters, R_0 increases, thus enhancing disease transmission.

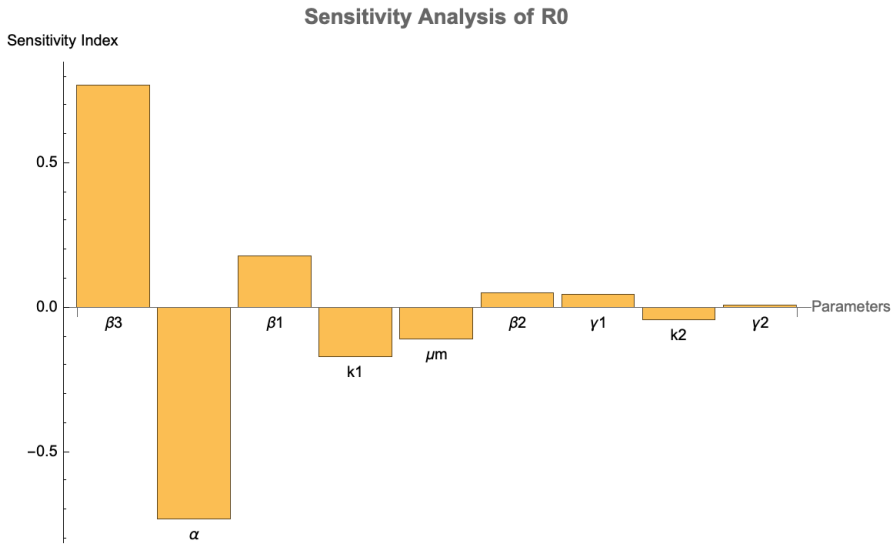

Figure 5: Sensitivity indices of R_0 with respect to different parameters of the model

Among these, β_3 exhibits the highest positive sensitivity, suggesting that transmission from the population under treatment contributes mainly to the spread of infection. This highlights the importance of strict infection control measures in healthcare and quarantine settings.

On the other hand, the recovery rate α and other removal-related parameters such as k_1, k_2, and μ_m show negative sensitivity indices. This indicates that increasing these parameters reduces R_0, thereby contributing to disease control. In particular, the recovery rate α demonstrates a strong negative influence, emphasizing the importance of effective treatment measures to mitigate the progression of the disease. To further investigate the impact of the most sensitive parameters, Figure 6 shows the variation of R_0 with respect to β_3, β_1, and α, with all other parameters kept fixed at their baseline values.

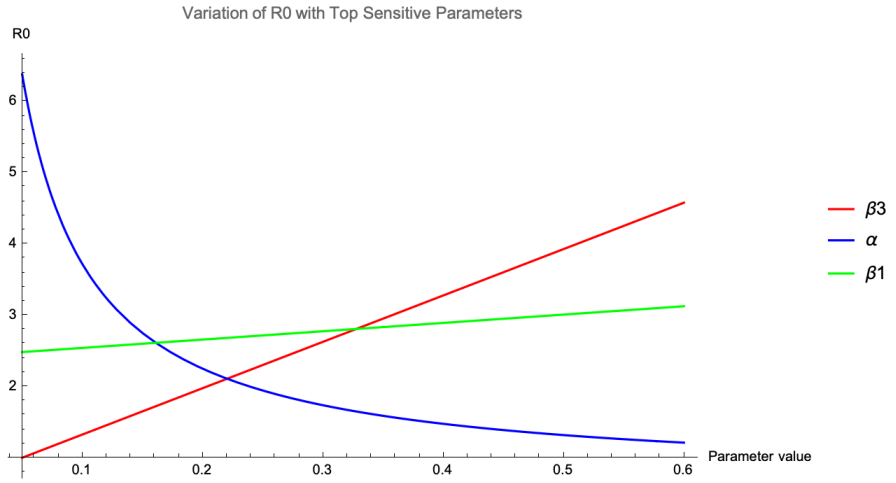

Figure 6: Variation of R_0 corresponding to the most sensitive parameters

It is observed that R_0 increases monotonically with increasing β_3 and β_1, confirming that higher transmission rates significantly enhance disease spread. In particular, the effect of β_3 is more pronounced, which is consistent with its higher sensitivity index.

Contrastingly, R_0 decreases sharply with increasing recovery rate α. This indicates that improving recovery through effective treatment can substantially reduce disease transmission. The steep decline of R_0 for smaller values of α suggests that obvious interpretation that low recovery rates would lead to rapid escalation of the infection.

These results validate the sensitivity analysis and demonstrate that controlling transmission rates and improving recovery are critical strategies for reducing the spread of COVID-19.

8. Conclusion

This study introduces a novel model employing an autonomous nonlinear system of ordinary differential equations in six time dependent variables to elucidate the progression of the virus causing infection for COVID-19. The model's analysis is centered on R_0, the reproduction number, a guiding parameter most commonly used to understand the dynamics of any infection. Stability analysis reveals that the D-F-E is both l.a.st as well as g.a.st when $R_0 \leq 1$. Also, for $R_0 > 1$, the E-E is likewise stable. Numerical simulations underscore the model's ability to depict disease dynamics accurately.

The sensitivity analysis indicates that R_0 is most influenced by the transmission parameter β_3 and the recovery rate α, with sensitivity indices 0.7705 and -0.7318 respectively. This indicates that transmission from the population under treatment, particularly the hospitalised infectives significantly accelerate disease spread. In contrast, obviously the higher recovery rates directly lead to reduction in infection levels.

Furthermore, the distinction between local and imported infections highlights the significant role of population mobility in regional disease dynamics, emphasizing the importance of monitoring and regulating movement across regions to prevent further outbreaks.

A significant insight from our research is the verification that once the virus enters a region, local transmission rates heavily influence its spread, complicating containment efforts, and leading to epidemic and pandemic conditions. Maintaining social distance, wearing masks and conducting widespread testing within the region need to be employed and executed more specifically. In addition, screening individuals entering the area can serve as a critical control measure.

Formulating an optimal control problem for this model and its mathematical analysis can be an interesting dimension to explore in further research.

Acknowledgment

The authors sincerely thank Naman Taggar for his technical support and assistance. The authors also express their gratitude to the reviewers for their constructive feedback and suggestions, which have greatly enhanced the clarity and impact of this research work.

References

[1] *The mathematical fractional modeling of tio-2 nanopowder synthesis by sol–gel method at low temperature.* 1

[2] Folashade B Agusto, Shamise Easley, Kenneth Freeman, and Madison Thomas, *Mathematical model of three age-structured transmission dynamics of chikungunya virus*, Computational and mathematical methods in medicine **2016** (2016), no. 1, 4320514. 3.1

[3] W Ahmad, MA Nazir, M Rafiq, AIK Butt, N Ahmad, and M Hussain, *Analyzing optimal control techniques in a nonlinear fractional rubella model with the atangana–baleanu derivative*, Computers in Biology and Medicine **197** (2025), 110954. 1

[4] W Ahmad, H Ullah, M Rafiq, AIK Butt, and N Ahmad, *Analytical and numerical investigations of optimal control techniques for managing ebola virus disease*, The European Physical Journal Plus **140** (2025), no. 4, 329. 1

[5] Waheed Ahmad, Muhammad Rafiq, Azhar Iqbal Kashif Butt, Momina Zainab, and Naeed Ahmad, *Dynamics of bi-susceptibility patterns in covid-19 outbreaks and associated abstain strategies*, Modeling Earth Systems and Environment **11** (2025), no. 3, 198. 1

[6] Waheed Ahmad, Muhammad Sultan Aslam, Muhammad Rafiq, Junaid Ahmad, and Ali Raza, *Modeling the impact of optimized treatment patterns on dengue transmission dynamics*, Chaos: An Interdisciplinary Journal of Nonlinear Science **35** (2025), no. 10. 1

[7] Ruchi Arora, Dharmendra Kumar, Ishita Jhamb, and Avina Kaur Narang, *Mathematical modeling of chikungunya dynamics: Stability and simulation*, Cubo (Temuco) **22** (2020), no. 2, 177–201. 4.4

[8] C. P. Bhunu, W. Garira, and Z. Mukandavire, *Modeling hiv/aids and tuberculosis coinfection*, Bulletin of Mathematical Biology **71** (2009), no. 7, 1745–1780. 5.2

[9] Sudhanshu Kumar Biswas, Jayanta Kumar Ghosh, Susmita Sarkar, and Uttam Ghosh, *Covid-19 pandemic in india: a mathematical model study*, Nonlinear Dynamics **102** (2020), no. 1, 537–553. 4.3

[10] Azhar Iqbal Kashif Butt, Tariq Ismaeel, Sara Khan, Muhammad Imran, Waheed Ahmad, IA Rashid, and Muhammad Sajid Riaz, *Investigating the role of antimalarial treatment and mosquito nets in malaria transmission and control through mathematical modeling*, Comput. Model. Eng. Sci. **144** (2025), no. 3, 3463–3492. 1

[11] Edmund X DeJesus and Charles Kaufman, *Routh-hurwitz criterion in the examination of eigenvalues of a system of nonlinear ordinary differential equations*, Physical Review A **35** (1987), no. 12, 5288. 4.3

[12] O Diekmann and JAP Heesterbeek, *Mathematical epidemiology of infectious diseases*, Model Building, Analysis (1989). 1

[13] Taruna Garg, Madhuchanda Rakshit, et al., *Analyzing pneumonia transmission with a fractional sveir model: the role of vaccination in disease eradication*, Discover Public Health **23** (2026), no. 1, 36. 1

[14] Taruna Garg, Madhuchanda Rakshit, M Manivel, and Shyamsunder, *Modeling of hepatitis b virus transmission with vaccination, treatment, and memory effects*, Advanced Theory and Simulations **9** (2026), no. 1, e01358. 1

[15] Delhi Government, *Annual report*, `http://des.delhigovt.nic.in/wps/wcm/connect/3b3bb3804949e070adc3bf26edbf4824/Annual+Report+2017.pdf?MOD=AJPERES&lmod=-1268218958&CACHEID=3b3bb3804949e070adc3bf26edbf4824&Annual%20report%20of%20Registration%20of%20Births%20and%20Deaths%20in%20Delhi%202017`.

[16] Herbert W. Hethcote, *The mathematics of infectious diseases*, SIAM Review **42** (2000), no. 4, 599–653. 1

[17] Manh Tuan Hoang, *A simple approach for studying stability properties of an seirs epidemic model*, Journal of Applied Analysis **31** (2025), no. 1, 143–156. 5.3

[18] Ruchi Kaur, Prabhanshi, Ishita Jhamb, and Pratibha Verma, *Transmission dynamics of covid-19 across a region: A mathematical model*, Proceedings of the National Academy of Sciences, India, Section A: Physical Sciences (2025), In press. 1, 2

[19] Ruchi Kaur, Naman Taggar, Vaishnavi Rajagopalan, and Jaspreet Kaur, *Mathematical modelling in epidemiology*, RESONANCE (2026), 45. 1

[20] Subhas Khajanchi, Kankan Sarkar, and Jayanta Mondal, *Dynamics of the covid-19 pandemic in india*, (2021).

[21] Gwenan M Knight, Thi Mui Pham, James Stimson, Sebastian Funk, Yalda Jafari, Diane Pople, Stephanie Evans, Mo Yin, Colin S Brown, Alex Bhattacharya, et al., *The contribution of hospital-acquired infections to the covid-19 epidemic in england in the first half of 2020*, BMC infectious diseases **22** (2022), no. 1, 556. 2

[22] Kok Yew Ng and Meei Mei Gui, *Covid-19: Development of a robust mathematical model and simulation package with consideration for ageing population and time delay for control action and resusceptibility*, Physica D: Nonlinear Phenomena **411** (2020), 132599. 3.2

[23] SD Purohit et al., *A novel study of the impact of vaccination on pneumonia via fractional approach*, Partial Differential Equations in Applied Mathematics **10** (2024), 100698. 1

[24] O Sadek, L Sadek, S Touhtouh, and A Hajjaji, *The mathematical fractional modeling of tio-2 nanopowder synthesis by sol–gel method at low temperature*, Math. Model. Comput **9** (2022), no. 3, 616–626. 1

[25] Piu Samui, Jayanta Mondal, and Subhas Khajanchi, *A mathematical model for covid-19 transmission dynamics with a case study of india*, Chaos, Solitons & Fractals **140** (2020), 110173. 5.1

[26] Nita H. Shah, Nisha Sheoran, Ekta Jayswal, Dhairya Shukla, Nehal Shukla, Jagdish Shukla, and Yash Shah, *Modelling covid-19 transmission in the united states through interstate and foreign travels and evaluating impact of governmental public health interventions*, Journal of Mathematical Analysis and Applications (2020), 124896. 1

[27] Shyamsunder and Manisha Meena, *A comparative analysis of vector-borne disease: monkeypox transmission outbreak*, Journal of Applied Mathematics and Computing **71** (2025), no. 4, 6119–6155. 1

[28] G.F. Simmons, *Differential equations with applications and historical notes*, Textbooks in Mathematics, CRC Press, 2016. 5.2

[29] Shakir Ullah, Imtiaz Ahmad, Mohammad Idrees, Saeed Islam, and Ishtiaq Ali, *Analysis of tuberculosis transmission dynamics with environmental and reinfection factors: a mathematical approach*, Journal of Applied Mathematics and Computing **72** (2026), no. 2, 86. 3.2

[30] WHO, *Covid-19 vaccines*, `https://www.who.int/emergencies/diseases/novel-coronavirus-2019/covid-19-vaccines`. 1